Clays and Clay Minerals, Vol. 62, No. 1, 35–52, 2014.

NATURAL CLAY-SIZED GLAUCONITE IN THE NEOGENE DEPOSITS OF THE CAMPINE BASIN (BELGIUM)

R. Adriaens*, N. Vandenberghe, and J. Elsen

Applied Geology and Mineralogy, Department of Earth and Environmental Sciences, University of Leuven, Celestijnenlaan 200E, 3000 Leuven, Belgium

Abstract—Natural clay-sized glauconite has the same mineralogical composition as sand-sized glauconite pellets but occurs in <2 μm clay fractions. This particular glauconite habit has been described previously from soil environments resulting from pelletal weathering but is rarely reported in higher-energy sedimentary environments. In the present study, clay-sized glauconite was identified as a common constituent in transgressive Neogene glauconite pellet-rich deposits of the southern North Sea in Belgium. X-ray diffraction results revealed that the characteristics of the clay-sized glauconite are very similar to the associated glauconite pellets in sand deposits. Both glauconite types consisted of two glauconite-smectite R1 phases with generally small percentages of expandable layers (<30%) with d_{060} values ranging between 1.513 Å and 1.519 Å. Clay-sized glauconite was not neoformed but formed by the disintegration of sand-sized glauconite pellets which were abraded or broken up during short-distance transport within the sedimentary basin or over the hinterland. Even in an environment where authigenic glauconite pellets occur, minimal transport over transgressive surfaces is sufficient to produce clay-sized glauconite. Furthermore, clay-sized glauconite can be eroded from marine deposits and subsequently resedimented in estuarine deposits. Clay-sized glauconite is, therefore, a proxy for the transport intensity of pelletal glauconite in energetic depositional environments and, moreover, indicates reworking in such deposits which lack pelletal glauconite.

Key Words—Belgium, Clay-sized Glauconite, Neogene, Transport.

INTRODUCTION

Authigenic glauconite is a sensitive indicator of low sedimentation rates in the marine realm and constitutes a powerful tool for sedimentological and sequence stratigraphic interpretations as well as K-Ar dating studies (Chamley, 1989; Amorosi, 1995; Hesselbo and Huggett, 2001; Potter *et al.*, 2005; El Albani, 2005; Harris *et al.*, 2007; Derkowski *et al.*, 2009). Many deposits contain transported glauconite pellets, which drastically changes the interpretation of environmental conditions during deposition (McRae, 1972; Odin and Matter, 1981; Cudzil and Dreise, 1987; Odin and Fullagar, 1988; Chafetz and Reid, 2000; Gonzalez *et al.*, 2004).

Physical transport of glauconite pellets leads to pellet abrasion, large amounts of fragmented particles (Amorosi, 1997; Udgata, 2007), or even complete disintegration of clay flakes resulting in the production of clay-sized glauconite material. This process has been identified in soils where the clay fraction consists predominantly of a glauconite mineralogy (Van Ranst and De Coninck, 1983; Tedrow, 1986, 2002).

Clay-sized glauconite in sedimentary rocks was suggested by Baioumy and Boulis (2012) to represent a pre-pelletal stage during glauconitization. Depending on its compositional and sedimentological characteristics, clay-sized glauconite has a transported origin, indicative of a rather high-energy environment or an authigenic origin, indicative of a lower-energy depositional environment. Clay-sized glauconite is, however, almost never reported in sedimentary deposits and certainly not co-existing with pelletal glauconite.

The current study documents the common presence of such clay-sized glauconite in Neogene glauconite-pellet-rich deposits of the southern North Sea in Belgium (Campine basin). First, experiments were performed to evaluate disintegration behavior of glauconite particles during several types of sample treatment. Second, a methodology was established to investigate the mineralogy of both glauconite pellets and associated clay-sized fractions. The study further addressed the relationship between sand-sized glauconite pellets and clay-sized glauconite, along with the origin and sedimentological significance of the latter.

CRITERIA TO IDENTIFY AND QUANTIFY GLAUCONITE MINERALS

Standard reference mineralogy and chemistry of glauconite pellets

The mineral glauconite is an Fe-rich dioctahedral mica which can be formed in various ways, with tetrahedral Al^{3+} or Fe^{3+} >0.2 atoms per formula unit and octahedral R^{3+} >1.2 atoms. A generalized formula is $K(R^{3+}_{1.33}R^{2+}_{0.67})(Si_{3.67}Al_{0.33})O_{10}(OH)_2$ with Fe^{3+} > Al and Mg > Fe^2 (Bailey,1980). The d_{060} values must be

* E-mail address of corresponding author:
rieko.adriaens@ees.kuleuven.be
DOI: 10.1346/CCMN.2014.0620104

>1.510 Å and K^+ should be the dominant interlayer cation (Bailey, 1988). The mineralogy of glauconite pellets, however, seldom consists of the pure glauconite mica. Instead, one or more Fe-rich mixed-layered glauconite-smectite phases are encountered (Buckley *et al.*, 1978; El Albani, 2005; Adriaens, 2009; Baldermann *et al*. 2012). Al-rich glauconite species were also reported by Berg-Madsen (1983) and Weaver and Pollard (1973), however. The composition of Al-rich glauconite overlaps with that of Fe-illite, which is related to non-marine environments (Meunier, 2005; Meunier and El Albani, 2007), although Banerjee *et al.* (2008) claimed the presence of Fe-illite in a marine succession. Nevertheless, marine Al-rich glauconite, or Fe-illite, is the result of diagenetic alteration (Odin and Matter, 1981; Ireland *et al.*, 1983) and neither is found in unlithified sediments. Consequently, illitic mineral species with >15 wt.% total Fe, which is expressed by d_{060} values >1.51 Å, are termed glauconite or glauconite-smectite here (Velde, 1985; Meunier, 2005).

Identifying and quantifying clay-sized glauconite in mixtures of clay minerals

As discussed above, the identification of glauconite minerals is based on both mineralogical and chemical data in cases of pure minerals. In clay-mineral mixtures, however, the situation is often much more complex and the use of chemical characterization methods is less straightforward. Deriving mineralogical information and parameters from X-ray diffraction (XRD) patterns combined with detailed XRD clay modeling is, therefore, the optimal working method.

As stated by Moore and Reynolds (1997), the cation size and site occupancy of the dominant octahedral trivalent cation correlates with the d_{060} peak position. Furthermore, when considering the general stability of the 060 area in terms of structural and chemical variations common for clays, this area represents a valuable and reliable tool in X-ray powder diffractometry to distinguish between different clay species (Środoń *et al.*, 2001). Consequently, the d_{060} values of different illitic 10 Å species are positioned at, or lower than, 1.500 Å for normal illite, between 1.500 Å and 1.510 Å for Fe-rich illite, and >1.510 Å for glauconite. This clear-cut differentiation can be obscured in mixtures of glauconite and nontronite which are rarely reported and absent from the present setting.

GEOLOGICAL SETTING

During the Neogene, sedimentation is restricted to the Campine area in the northern part of Belgium (Figure 1).

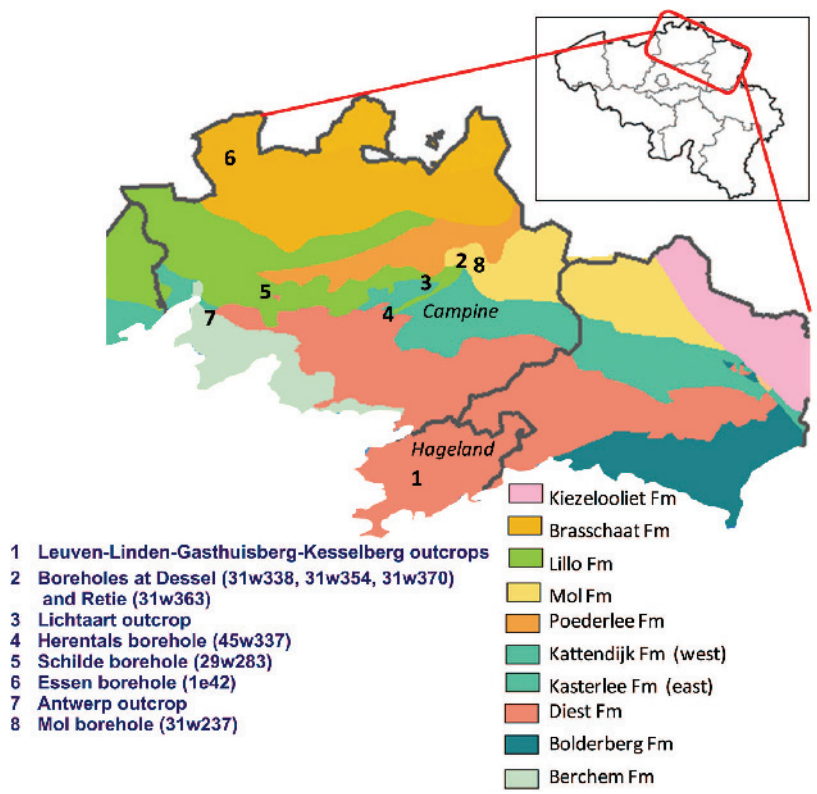

Figure 1. Geographical locations of out-crop or bore-hole samples plotted on the Tertiary geological map of the northern part of Belgium. The out-cropping formations presented here are indexed at the bottom right. Bore-hole codes correspond to codes of the Belgian Geological Survey.

https://doi.org/10.1346/CCMN.2014.0620104 Published online by Cambridge University Press

Figure 2. (left) Glauconitic sands of the Diest Formation intercalated with thin, irregular clay layers. (right) Slightly glauconitic sands of the Kasterlee Formation with thin clay intercalations.

Deposits are mainly transgressive shallow-marine glauconite-rich sands but minor estuarine to fluvial sand deposits occur also (Vandenberghe *et al.*, 1998; 2004). Clay in these deposits occurs dispersed in the sand matrix and as thin intercalated clay layers (Figure 2). Depositional sequences are separated by erosion surfaces, interpreted as major stratigraphic unconformities. The chronostratigraphic position of the different units is based on Vandenberghe *et al.* (1998) and Louwye *et al.* (2000) (Table 1).

The Early Miocene sands of the Berchem Formation are subdivided in the Burdigalian Edegem and Kiel sand Members and the Langhian-Serravalian Antwerp sand Member (De Meuter and Laga, 1976), which were all deposited in a fully marine environment (De Meuter and Laga, 1976; Louwye and Laga, 1998; Louwye, 2001). These three members are fine- to medium-grained sand units commonly intercalated with thin clay layers (Vandenberghe *et al.*, 1998; Louwye *et al.*, 2000; Louwye, 2005). Distinction is made based on calcareous fossils, dinoflagellate biozonations, and glauconite contents (Table 1). Radiometric glauconite dating led Odin *et al.* (1974) to conclude an authigenic origin for the Antwerp glauconites while the Edegem and Kiel glauconites are considered to be reworked.

After an important phase of erosion, sedimentation only restarted in the latest Serravalian–early Tortonian with the Diest Formation (Louwye *et al.*, 1999). This poorly sorted sand unit occurs in both the Hageland and the Campine area with average glauconite contents of

Table 1. Stratigraphical overview of the Neogene units investigated in the present study, their average pelletal glauconite contents, and the potential of each unit to contain authigenic glauconites.

Chronostratigraphy	– Lithostratigraphic unit – Formation	Member	Average Gl content	Authigenic Gl potential
Zanclean/ Piacenzian	Mol Formation / Poederlee Formation		<0.01% / 20%	very low / medium
Messinian	Kasterlee Formation		3%	very low
Tortonian	Diest Formation		39%	very low
Serravallian				
Langhian	Berchem Formation	Antwerp Member	50%	medium
Burdigalian		Kiel Member	35%	low
		Edegem Member	35%	low

https://doi.org/10.1346/CCMN.2014.0620104 Published online by Cambridge University Press

40% (Figure 1 and Table 1). Discontinuous clay layers are commonly observed in these sands (Figure 2). The Diest sands in the Hageland area contain no microfossils, which makes their exact stratigraphic positioning questionable.

The Late Miocene Kasterlee Formation was formed in a near-shore depositional environment or embayment with a manifest river discharge and was, thus, influenced by oxic freshwaters (Louwye, 2005; Louwye *et al.*, 2006). This resulted in a well sorted, fine-grained sand unit with thin irregular clay intercalations (Figure 2). Glauconite contents in the Kasterlee Formation are typically much smaller than the older Miocene sand deposits, with typical values of only 5%.

The Pliocene Poederlee sand is a fine glauconitic sand unit with disperse clay lenses (De Meuter and Laga, 1976) often presented as highly oxidized sands with a hard limonitic crust. Louwye and De Schepper (2010) suggest a near-coastal, possibly shoaling environment, with more terrestrial influence in the upper part of the formation. Glauconite contents in the Poederlee sands are variable, ranging from 5 to 30%.

A thick unit of continental to estuarine sands of the Mol Formation occurs geographically more to the east (Figure 1). This unit consists of very quartz-rich glass sands with very small clay contents and contains virtually no glauconite pellets.

Under a binocular microscope, glauconite pellets in the sand units described above generally appear pale to dark green, with the latter variety occurring more frequently. Pellets are often well rounded and polished but also more irregular pellet shapes occur. Cracks in pellets and broken fragments are commonly observed (Figure 3). The spatial distribution of glauconite pellets is often very irregular as they occur concentrated in cross beds, on transgressive surfaces, and in basal green sands but also dispersed in the sand matrix. When mixed with water, the suspension water of sand deposits displays a pronounced green coloration. However, the suspension water of sedimentary clay is grey to brown colored and rarely contains any glauconite pellets.

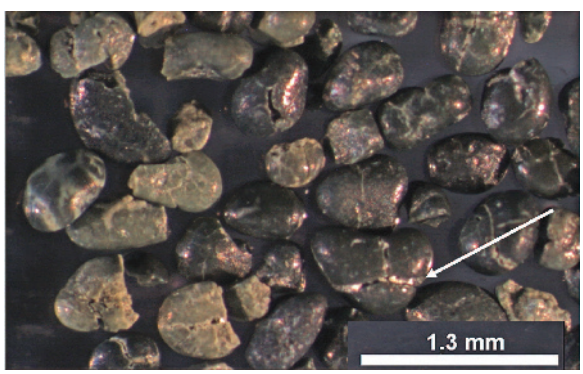

Figure 3. Glauconite pellets of the Kasterlee Formation. Pellets occur very regularly as fragmented or broken pieces. Rims are sometimes filled with clay precipitates as indicated by the arrow.

The relation in terms of size distribution of glauconite pellets to the remainder of the sediments reveals important information regarding possible mutual transport (Figure 4). For the formations of Diest and Kasterlee, and the Edegem and Kiel Members of the Berchem Formation, both distributions are very similar, which confirms simultaneous transport of glauconites and detrital particles. In contrast, the Poederlee Formation and the Antwerp sands of the Berchem Formation contain potential authigenic glauconites. Their glauconite pellet distribution is differently shaped from the remaining fraction of the sediment and the glauconite pellets are significantly larger than the remainder of the sediments (Figure 4). A reasonable conclusion is that the Neogene sediments in Belgium contain transported glauconites as well as possible authigenic glauconite horizons. These sediments are ideal, therefore, to test the presence of clay-sized glauconite and investigate the possible relation between glauconite pellets and the associated clay fraction.

DISINTEGRATION EXPERIMENTS ON GLAUCONITE PELLETS

Clay-sized glauconite might be artificially introduced into clay fractions during sampling or laboratory-preparation procedures. In order to verify such artificial contributions, the effects of different preparation processes were evaluated experimentally.

A first experiment was set up to investigate the effect of commonly applied geological lab procedures such as washing, shaking, stirring, wet sieving, and oven drying. This type of preparation procedure caused minimal disintegration of glauconites as contaminants were either absent or undetectable. Nevertheless, sample suspensions which were subjected to high-speed shaking for >24 h demonstrated a slightly greener coloration, illustrating that glauconite pellets broke up during this last procedure.

In a second experiment, purified >32 μm glauconite pellets of Neogene deposits were subjected to the standard clay preparation treatment for aggregate removal (modified after Jackson, 1975). The >32 μm glauconite pellets were separated paramagnetically from a washed and sieved sand sample and subjected to heating in a Na-acetate-buffer solution, H_2O_2, and Na-dithionite in a Na-citrate+$NaHCO_3$-solution (modified after Jackson, 1975; Zeelmaekers, 2011). The amount of disintegrated <2 μm pellets was determined quantitatively by weight. Based on 12 samples, the amount of clay produced from decomposed pellets averaged between 15 and 25 wt.%. Although this experiment was on purified glauconite pellets, it showed clearly that significant errors can be induced when glauconite pellets are not removed before standardized clay-preparation procedures.

https://doi.org/10.1346/CCMN.2014.0620104 Published online by Cambridge University Press

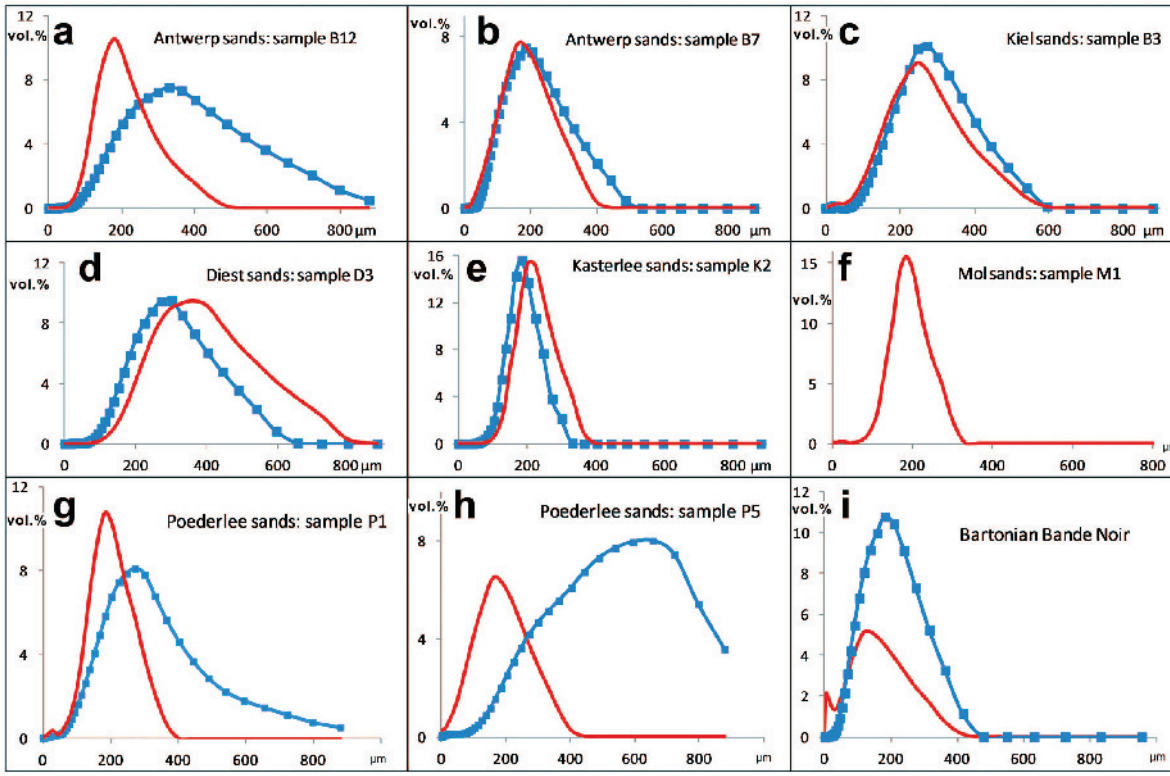

Figure 4. Comparison of the particle-size distribution between the >32 µm glauconite fraction (dotted blue) and the rest (red). The Poederlee (g,h) and Antwerp sands (a,b) typically contain large glauconite pellets with a particular size distribution, suggesting potential authigenic glauconitization. The pellet size is less well sorted than might be expected for authigenic minerals, *e.g.* the Bartonian Bande Noir horizon (I) (Odin, 1982; Maréchal, 1994). Some samples of the Antwerp and Poederlee sand (b, g) have similar particle-size distributions for quartz and glauconite, suggesting a common transport history.

A third experiment was set up to study contamination by glauconite particles in the 2–32 µm size fraction. Untreated samples were split into two parts and soaked in water. The first part was centrifuged to remove the <2 µm size fraction without any treatment, then the amounts of glauconite in the <2 µm and >2 µm size fractions were determined. To the second split, the standard clay treatments were applied (see second experiment). The <2 µm and >2 µm size fractions were then separated by centrifugation and the amount of glauconite was determined in both.

Two main observations can be made from this experiment. Firstly, large amounts of glauconite occurred in the <2 µm size fraction of untreated samples (Figure 5). Secondly, the increase in artificially produced <2 µm glauconite particles after treatment was limited to 15–20 wt.% (Figure 5). Nevertheless, this must be a maximum value because, due to the applied treatment, some clay aggregates also shifted to the <2 µm size fraction.

During a fourth experiment, a fresh clay outcrop sample of the Bartonian Bande Noir horizon (Maréchal, 1994) containing large amounts of glauconite pellets was subjected to several destructive actions such as shovel cutting, pushing, and shearing. The clay suspension immediately adopted a much greener color compared with the untreated sample. The <2 µm clay fraction was centrifuged before and after the destructive actions and analyzed using bulk XRD methods. The results indicated that, while the clay fraction of the untreated sample contained 20 wt.% glauconite, the treated sample had 30 wt.% glauconite in its clay fraction.

Consequently, the application of routine laboratory procedures affects glauconite particles in these sediments to such a degree that clay-sized glauconite is formed. However, these introductory experiments demonstrated that large amounts of <2 µm glauconite particles occur naturally in the clay fraction. After laboratory treatments, the amount of clay-sized glauconite increased to 20% at most, indicating that the majority of clay-sized glauconite occurs naturally.

SAMPLES AND METHODS

A selection of samples from the formations of Berchem, Diest, Kasterlee, Poederlee, and Mol were studied for glauconite pellet mineralogy and associated clay mineralogy. Samples were collected in various available cores and outcrops (Table 2, Figure 1).

https://doi.org/10.1346/CCMN.2014.0620104 Published online by Cambridge University Press

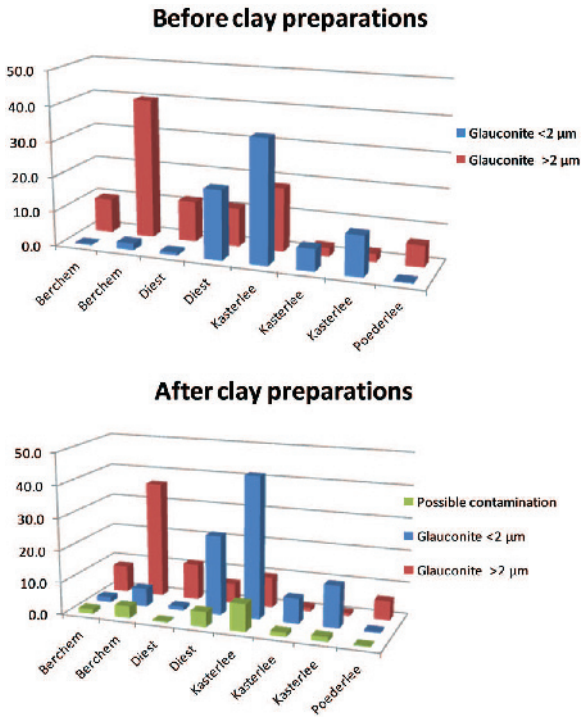

Figure 5. Results of the glauconite pellet disintegration experiment. Untreated samples were centrifuged with a Thermo Scientific SL40R benchtop centrifuge (relative centrifugal force $25214 \times g$ –Thermo Fisher Scientific, Erembodegem, Belgium) to <2 µm to quantify the amount of glauconite minerals present in the finer and coarser size fractions. This procedure was repeated after applying the standard clay-preparation procedures. The columns in green correspond to the maximum possible amount of contamination of >2 µm glauconite material that ended up in the <2 µm clay fraction.

Considering the importance of glauconite pellet disintegration behavior as demonstrated in the section above, the >32 µm glauconite pellets were separated systematically from the remainder of the sediment. Sand samples were soaked in demineralized water, stirred, and separated by 32 µm wet sieving, which was repeated three times. Glauconite pellets were isolated from the >32 µm fraction using a Frantz isodynamic magnetic separator. Clay samples were not treated because they contained no glauconite pellets. Both clay samples and <32 µm fractions of sand samples were examined for bulk mineralogy as well as for clay mineralogy on clay slides. Bulk measurements were recorded with XRD from randomly oriented powders which were fine-milled and mixed with an internal standard (after Środoń *et al.*, 2001). Oriented clay slides were prepared after the removal of all aggregate-forming particles (modified after Jackson, 1975; Zeelmaekers, 2011), followed by centrifugation of the <2 µm fraction. The clay material was subsequently Ca-saturated to ensure homogenous swelling of smectitic components (Eberl *et al.*, 1987; Sakharov *et al.*, 1999), and oven-dried afterward at 60ºC. Clay (<2 µm) material was also analyzed as randomly oriented powders by XRD, analogous to the procedure applied for bulk samples (after Środoń *et al.*, 2001).

Glauconite pellets were examined for mineralogy by XRD as randomly oriented powders but also as oriented slides after fine milling and subsequent Ca saturation. The major-element chemistry of glauconite pellets was characterized using inductively coupled plasma-optical emission spectroscopy (ICP-OES) while ferrous iron was determined through titration (after Wilson, 1955).

All XRD measurements were carried out at the department of Earth and Environmental Sciences at the University of Leuven on a Phillips PW1830 with CuKα radiation at 30 mA and 45 kV using a graphite monochromator and a scintillation detector. Diffractometer scans were recorded in Bragg-Brentano geometry from 5 to 65º for bulk measurements and from 2 to 47º for clay measurements, each time with a step size of 0.02º and 2 s counting time per step. Oriented slides were measured under air-dry, glycolated, and heated (550ºC) conditions.

Quantification of the <2 µm clay fraction was done in two independent ways. Firstly, clay modeling using the software *Sybilla* (©Chevron ETC) was used for interpretation, clay-structure analysis, and quantification. Secondly, quantification of randomly oriented powders and characterization of the 060 area was performed using the software *Quanta* (©Chevron ETC). This full-pattern fitting software bases the clay mineral quantification on the integrated intensity of the 060 area. The efficiency and accuracy of this method was described previously (Środoń *et al.*, 2001; Kleeberg, 2005; Omotoso *et al.*, 2006). Furthermore, the method takes advantage of the fact that clay mineral species with different 060 spacings can be quantified separately, which makes it ideally suited for independent glauconite quantification in the presence of the more common Al-rich clay mineral species.

RESULTS

Glauconite pellets

An inventory of mineralogical characteristics and chemical compositions of the glauconite-pellet bearing horizons in the Upper-Cretaceous and Cenozoic in Belgium was reported by Adriaens (2009). Cretaceous glauconite-bearing horizons were characterized by a 1*M* to 1*Md*-glauconite-smectite R1 phase with expandable layers ranging between 6 and 8%. Throughout the Cenozoic record, glauconite pellet mineralogy displays low variability, consisting of one or two 1*Md*-glauconite-smectite R1 phases with <16% expandable layers in total. Neogene glauconite pellets, from similar stratigraphic horizons to those used in the present study, typically contain between 6 and 12% expandable layers. The position of the 060 reflection of these glauconite pellets varied between 1.515 Å and 1.519 Å. Major-element analysis by ICP-OES revealed K_2O contents

https://doi.org/10.1346/CCMN.2014.0620104 Published online by Cambridge University Press

Table 2. Overview of samples with information regarding stratigraphy, origin, and lithology. Borehole and outcrop locations are shown in Figure 1.

Name	Formation	Member	Location	Lithology	State
B1	Berchem	Edegem	Kruibeke claypit outcrop	Sand	Fresh
B2	Berchem	Kiel	Schilde borehole 66.3 m	Sand	Fresh
B3	Berchem	Kiel	Schilde borehole 67.3 m	Sand	Fresh
B4	Berchem	Kiel	Antwerp outcrop	Sand	Fresh
B5	Berchem	Kiel	Schilde borehole 64.8 m	Sand	Fresh
B6	Berchem	Antwerp	Herentals borehole 75.5 m	Sand	Fresh
B7	Berchem	Antwerp	Herentals borehole 85.5 m	Sand	Fresh
B8	Berchem	Antwerp	Dessel 5 borehole 165.5 m	Clay	Fresh
B9	Berchem	Antwerp	Dessel 5 borehole 165.9 m	Clay	Fresh
B10	Berchem	Antwerp	Essen borehole 176.9 m	Sand	Fresh
B11	Berchem	Antwerp	Mol borehole 143.7 m	Sand	Fresh
B12	Berchem	Antwerp	Essen borehole 180.5 m	Sand	Fresh
B13	Berchem	Antwerp	Schilde borehole 62.8 m	Sand	Fresh
D1	Diest (Campine)		Essen borehole 172.5 m	Sand	Fresh
D2	Diest (Campine)		Essen borehole 174.6 m	Sand	Fresh
D3	Diest (Campine)		Essen borehole 175.9 m	Sand	Fresh
D4	Diest (Campine)		Retie 1 borehole 48.86 m	Sand	Slightly oxidized
D5	Diest (Campine)		Dessel 2 borehole 47.50 m	Sand	Slightly oxidized
D6	Diest (Campine)		Dessel 2 borehole 34.65 m	Clay	Fresh
D7	Diest (Hageland)		Leuven GHB outcrop	Sand	Slightly oxidized
D8	Diest (Hageland)		Linden outcrop	Sand	Slightly oxidized
D9	Diest (Hageland)		Leuven Kesselberg outcrop	Sand	Slightly oxidized
D10	Diest (Hageland)		Leuven GHB outcrop	Sand	Slightly oxidized
D11	Diest (Hageland)		Leuven GHB outcrop	Clay	Fresh
D12	Diest (Hageland)		Leuven GHB outcrop	Clay	Fresh
K1	Kasterlee		Dessel 3 borehole 28.58 m	Sand	Fresh
K2	Kasterlee		Dessel 3 borehole 29.78 m	Sand	Fresh
K3	Kasterlee		Dessel 2 borehole 32.03 m	Sand	Fresh
K4	Kasterlee		Lichtaart outcrop	Sand	Fresh
K5	Kasterlee		Lichtaart outcrop	Sand	Fresh
K6	Kasterlee		Dessel 3 borehole 30.73 m	Clay	Fresh
K7	Kasterlee		Dessel 2 borehole 32.75 m	Clay	Fresh
M1	Mol		Dessel 3 borehole 12.10 m	Sand	Fresh
M2	Mol		Dessel 3 borehole 12.75 m	Sand	Fresh
M3	Mol		Dessel 3 borehole 13.10 m	Sand	Fresh
M4	Mol		Dessel 2 borehole 16.5 m	Sand	Fresh
M5	Mol		Dessel 2 borehole 19.2 m	Sand	Fresh
P1	Poederlee		Rees borehole 21.20 m	Sand	Fresh
P2	Poederlee		Rees borehole 21.55 m	Sand	Fresh
P3	Poederlee		Rees borehole 21.90 m	Sand	Fresh
P4	Poederlee		Rees borehole 22.40 m	Sand	Fresh
P5	Poederlee		Rees borehole 23.80 m	Sand	Fresh
P6	Poederlee		Rees borehole 24.20 m	Sand	Fresh

ranging from 5.5 to 7 wt.%, pointing to well evolved pelletal maturity (Table 3). Total (Fe_2O_3+FeO) contents for Neogene glauconite pellets ranged between 16 and 23.5 wt.% oxides (Table 3), with a typical ferric:ferrous ratio of 9:1, plotting within the glauconite compositional field of Meunier and El Albani (2007) (Figure 6).

The results of the clay modeling of oriented slides (Figure 7) show that the majority of analyzed glauconite pellets consisted of two separate phases: a glauconite-smectite R1 phase with 5–10% expandable layers and a three-component glauconite-expandable R1 phase with a total of 25–35% expandable layers of two types. The expandable minerals in the former phase are smectites of the low-charge type while in the three-component system they consist of both low-charge and high-charge smectite with a 60:40–70:30 ratio, respectively. Traces of kaolinite were often encountered as the result of clay precipitation in the pelletal rims (Figure 3). The glauconite pellets of the different investigated formations were characterized based on the relative amounts of both glauconite-expandable phases and their typical 060 value (Figure 7 and Table 4). Furthermore, during modeling, the octahedral Fe content of the glauconite pellets was assessed. This parameter shows low variability for all glauconite pellets investigated, ranging from 0.75 to 0.9/half unit cell.

https://doi.org/10.1346/CCMN.2014.0620104 Published online by Cambridge University Press

Glauconite pellets of the Berchem Formation typically display a 75:25 ratio between the less expandable two-component and more expandable three-component glauconite-smectite phase, respectively. No distinction was found between glauconite pellets of the Antwerp sand and the Kiel and Edegem sands. Glauconite pellets of both the Diest and Kasterlee Formations generally have a small amount of expandable layers, which was reflected in their 90:10 less expandable-more expandable ratio. Glauconite pellets of the Poederlee sands contained two R1 glauconite-smectite phases but also Fe-rich smectite was also present (Figure 7), which is unique in the Campine basin (Adriaens, 2009). The estuarine Mol Formation contained no glauconite pellets and was, therefore, not characterized further.

Clay mineralogy of the <2 μm fraction

Sands. The quantitative mineralogical composition of the <2 μm clay fractions from the sands, as determined by clay modeling (Figure 8), illustrates the systematic presence of clay-sized glauconite-smectite, which was defined by its unique 060 value and modeled octahedral Fe content (Figure 9, Table 4). Optimal modeling results were only obtained after introducing similar glauconite-smectite R1 phases which make up the mineralogy of the associated sand-sized glauconite pellets. The clay mineralogy of the Berchem Formation was always rich in discrete dioctahedral smectite and Al-rich mixed-layer illite-smectite. Clay-sized glauconite was quantified in total amounts ranging from 10% up to 30% with typically the more expandable type (three-component glauconite-smectite R1 with 22–30% expandable layers) dominating the less expandable type (glauconite-smectite R1 with 8−12% expandable layers) (Table 4 and Figure 8). Clay minerals in the Antwerp Member were not significantly different from those in the Edegem and Kiel Members. Sample B11, however, contained almost no clay-sized glauconite. In the Diest sands, the <2 μm clay mineralogy depended on the origin of the samples. Samples from the Hageland area contained large amounts of clay-sized glauconite, up to 90% of the total <2 μm fraction, with smaller amounts of Al-rich illite-smectite, illite, kaolinite, and, occasionally some chlorite. Diest sand samples originating from the Campine area, contained smaller amounts of clay-sized glauconite with values between 20 and 45%. Contributions from other clay minerals were, therefore, more important, in particular of discrete smectite, which is seldom found in sands in the Hageland area. Very similar more and less expandable clay-sized glauconite types as for the Berchem sands were used during modeling. In the Hageland area the less expandable type predominates, whereas in samples of the Campine area the ratio of more expandable type:less expandable type was just 2:1 (Table 4).

The Kasterlee sands contained variable amounts of clay-sized glauconite, ranging from 20 to 50%, with the less expandable clay-sized glauconite type generally dominating the more expandable type. While the kaolinite content in the Berchem and Diest sands was rather small (<10%), it was much greater in the Kasterlee sands with values between 15 and 35%.

Clay-sized glauconite also exists naturally in the Poederlee sands, but in limited amounts (<15%). Both the less and more expandable glauconite types were used in these clay patterns. Smectite was, however, the dominant clay mineral consisting of dioctahedral as well as trioctahedral expandable phases. The dioctahedral smectite is comparable in all formations discussed and appears to be very poor in Fe content, with the modeled octahedral Fe content <0.25/half unit cell. The trioctahedral expandable species was, however, very rich in Fe with 1.5 octahedral Fe/half unit cell.

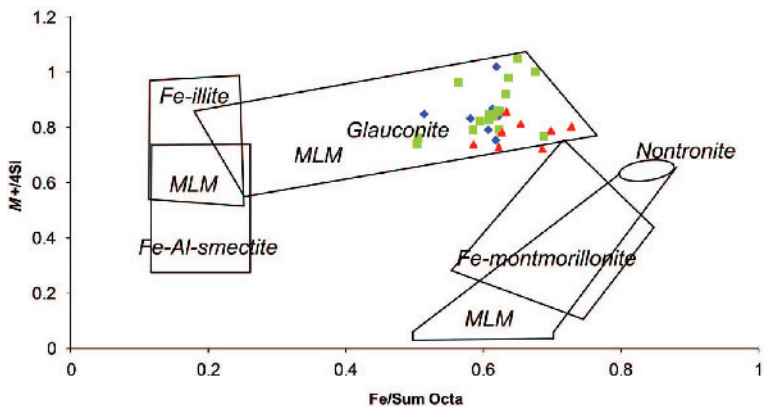

Figure 6. Position of the Belgian Cenozoic glauconite pellets (see Table 2 for sample information) in a compositional diagram. End-member positions are indicated by squares. MLM indicates mixed-layer minerals, *M*+ corresponds to the interlayer charge, while 'Sum octa' corresponds to the sum of octahedral cations in the structure. Blue dots refer to poorly expandable glauconite pellets (K_2O <7%), red triangles to pellets which are more expandable (K_2O >10%), and green squares to a group of glauconite pellets which expand to a medium extent (7%<K_2O<10%). Neogene glauconite pellets as presented here belong to the blue and green markers (modified after Meunier and El Albani, 2007).

https://doi.org/10.1346/CCMN.2014.0620104 Published online by Cambridge University Press

Table 3. Bulk chemical data (%) of Neogene glauconite pellets, analyzed using ICP-OES.

Chronostratigraphy		Chemical phase / Lithostratigraphy	SiO_2 0.01	Al_2O_3 0.01	Fe_2O_3 0.01	FeO 0.01	MgO 0.01	CaO 0.01	Na_2O 0.01	K_2O 0.01	MnO 0.001	TiO_2 0.001	P_2O_5 0.01
Neogene	Zanclean	Luchtbal sand	43.990	9.940	19.103	1.660	3.010	0.361	0.130	6.340	0.047	0.856	0.190
		Kattendijk sand	44.250	9.860	20.292	1.480	3.030	1.098	0.140	6.450	0.019	0.346	0.200
	Messinian	Kasterlee sand	44.080	12.810	15.631	1.480	2.450	0.403	0.140	5.520	0.015	0.492	0.120
		Kasterlee sand	49.150	10.200	21.570	1.300	2.950	0.479	0.140	6.260	0.012	0.317	0.100
	Tortonian	Diest sand	45.110	10.690	18.620	2.740	2.790	0.397	0.100	6.190	0.019	0.500	0.170
		Diest sand	46.890	9.490	19.770	2.210	3.120	0.386	0.130	6.950	0.007	0.161	0.110
		Diest sand	46.230	10.510	19.920	2.560	3.050	0.413	0.090	6.960	0.009	0.214	0.120
		Deurne sand	46.850	9.770	20.280	1.840	3.370	0.500	0.110	6.720	0.016	0.127	0.260
		Deurne sandstone	45.810	9.870	14.580	2.370	3.420	0.242	0.140	6.230	0.018	0.225	0.320
	Langhian	Zonderschot sands	45.440	8.670	20.270	3.270	3.190	1.317	0.210	6.400	0.021	0.288	0.170
		Antwerp sands	50.340	12.560	18.590	3.090	3.350	1.634	0.220	6.430	0.027	0.538	0.150
		Antwerp sands	44.110	9.510	18.800	2.730	3.050	0.847	0.150	6.320	0.012	0.174	1.270
		Antwerp sands	46.055	10.220	19.670	2.550	3.160	0.497	0.290	6.500	0.014	0.225	0.300
	Burdigalian	Kiel sands	45.160	9.680	13.550	2.550	3.170	2.548	0.200	6.090	0.010	0.164	0.070
		Kiel sands	47.350	9.990	20.370	2.200	3.070	0.370	0.130	6.550	0.010	0.218	0.260
		Kiel sands	45.580	9.840	18.270	2.190	3.020	3.290	0.130	5.960	0.011	0.217	0.260
		Kiel sands	46.983	9.580	17.710	3.090	3.450	0.300	0.130	6.600	0.009	0.147	0.160
Paleogene	Rupelian	Eigenbilzen sands	46.190	9.760	20.810	1.660	3.080	0.481	0.110	6.120	0.058	0.000	0.450
	Bartonian	base Asse-Ursel	43.040	6.650	14.030	3.480	2.450	0.485	0.190	5.850	0.011	0.146	0.050
		base Asse-Ursel	43.060	8.770	16.300	3.270	2.740	0.415	0.220	6.130	0.011	0.150	0.050
		Bande Noir	45.160	8.890	21.970	1.300	3.540	0.531	0.110	6.160	0.045	0.407	0.060
		Bande Noir	38.880	5.440	8.350	1.310	3.180	0.684	0.210	5.560	0.018	0.241	0.020
		Wemmel sands	42.300	8.070	19.530	1.840	3.700	1.451	0.130	6.070	0.227	0.439	0.060
		Wemmel sands	43.058	8.860	21.020	2.560	3.660	0.040	0.130	5.860	0.092	0.000	0.050
	Lutetian	Lede sands	42.688	8.910	12.270	2.210	2.940	0.671	0.110	4.990	0.130	0.000	0.030
		Brussel sands (Gobertange)	47.720	8.530	19.230	1.660	4.300	0.438	0.140	6.850	0.014	0.116	0.070
		Brussel sands (Gobertange)	48.840	8.380	20.930	1.660	4.260	0.691	0.130	6.960	0.019	0.105	0.060
		Brussel sands (Gobertange)	46.020	8.250	11.683	1.490	4.010	0.438	0.100	6.490	0.019	0.120	0.040
		Aalter sands	49.420	8.860	21.430	1.480	3.670	0.657	0.140	5.650	0.051	0.787	0.140
	Ypresian	Vlierzele sands	47.460	8.520	21.180	1.120	3.490	0.718	0.160	5.850	0.026	0.259	0.070
		Vlierzele sands	44.110	9.410	11.757	0.760	2.670	0.626	0.140	4.570	0.027	0.188	0.110
		Vlierzele sands	49.530	9.510	19.907	1.120	3.020	0.775	0.180	5.620	0.021	0.209	0.050
		Vlierzele sands	49.690	7.860	21.112	1.130	3.130	1.281	0.180	5.950	0.026	0.158	0.060
		Bierbeek sands	44.570	12.440	15.250	2.200	2.830	1.076	0.230	3.710	0.081	2.171	0.110
		Egem sandstone	47.560	6.950	22.190	2.730	3.360	0.556	0.140	6.230	0.031	0.358	0.110
	Thanetian	Tuffeau de Lincent	47.270	7.320	20.150	0.760	3.290	0.846	0.110	6.230	0.137	0.201	0.110
Cretaceous	Campanian	Vaals sands	48.090	7.460	24.350	1.300	2.450	0.764	0.140	6.100	0.013	0.119	0.180
	Santonian	Chalky sandstone	49.400	7.400	19.220	2.560	3.980	0.760	0.310	8.140	0.007	0.063	0.420
	Coniacian	Craies de Maisières	46.840	9.450	16.570	1.480	3.770	0.068	0.190	7.400	0.006	0.073	2.150
	Turonian	Dièves marls	43.000	6.880	5.730	2.560	3.460	1.212	0.120	6.630	0.009	0.074	0.350

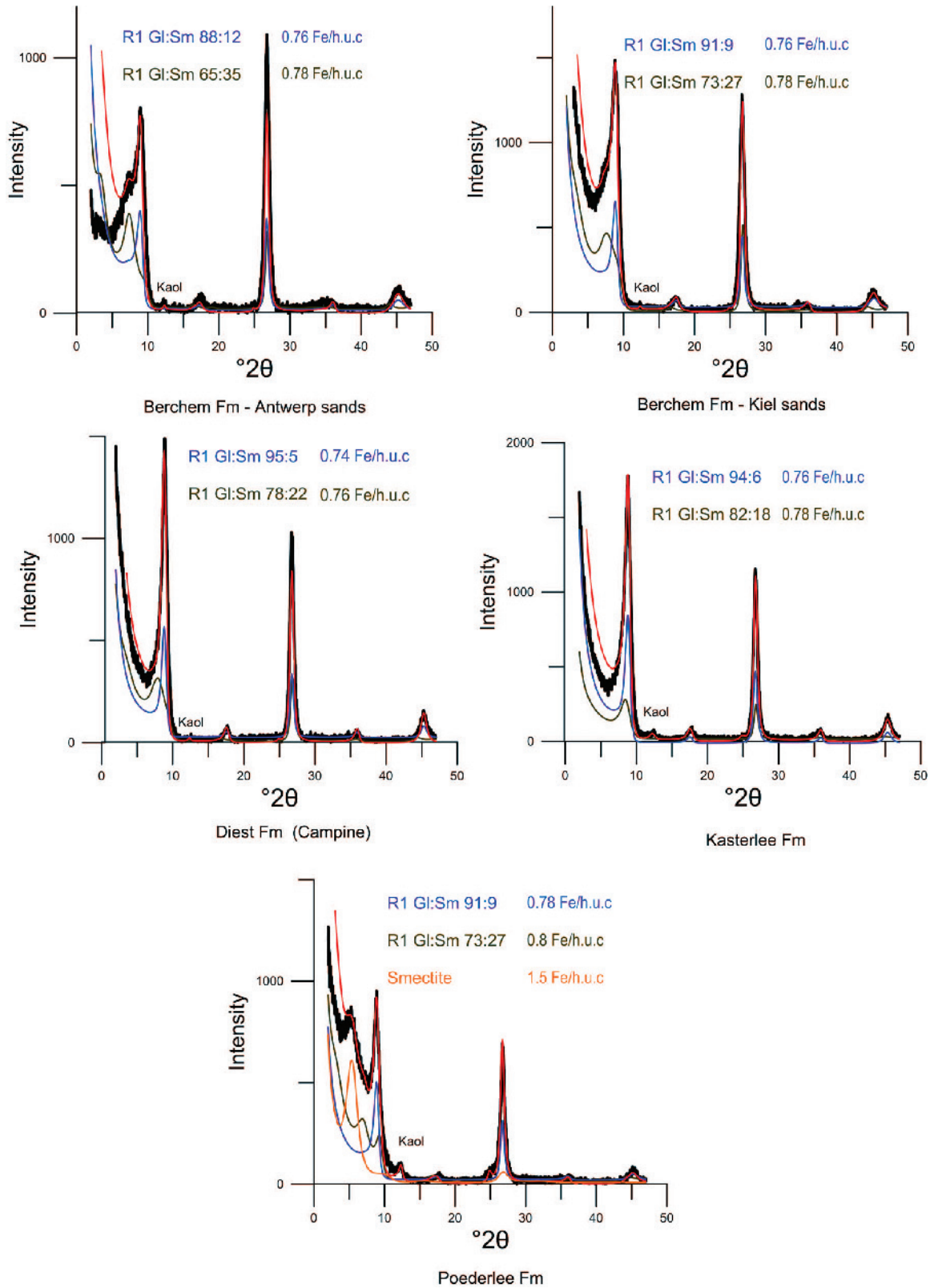

Figure 7. XRD traces of glauconite pellets glycolated (black) and the Sybilla-fitted model (red) . The glauconite-smectite R1 phases used in the clay modeling are shown in blue and green for each formation and are representative of all studied samples. 'Kaol' indicates small amounts of kaolinite.

https://doi.org/10.1346/CCMN.2014.0620104 Published online by Cambridge University Press

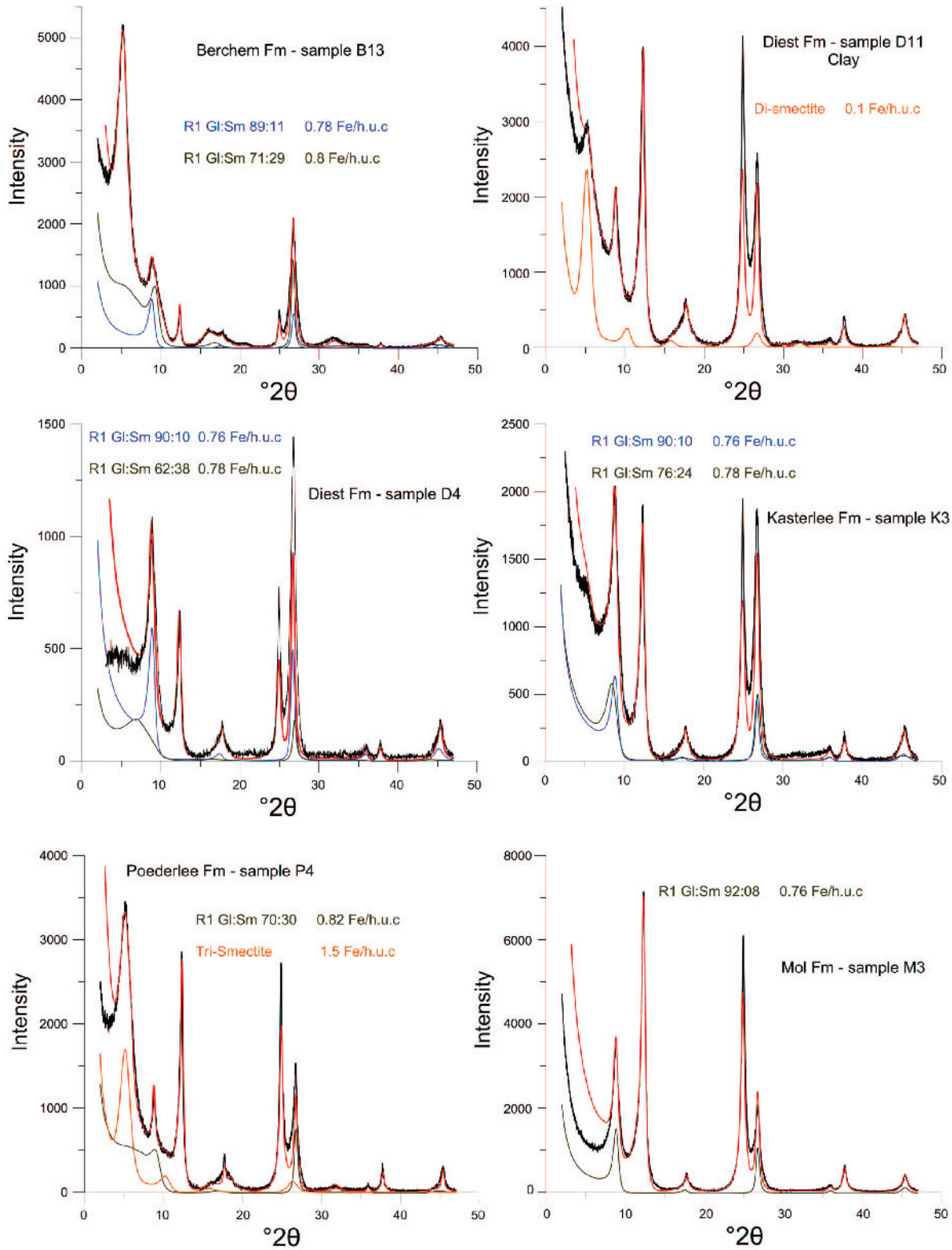

Figure 8. XRD traces of Ca-saturated clay fractions (<2 μm, glycolated, on oriented slides) (black). The Sybilla model fit is shown in red. The glauconite-smectite R1 phases used in the clay modeling are shown in blue and green for each formation.

https://doi.org/10.1346/CCMN.2014.0620104 Published online by Cambridge University Press

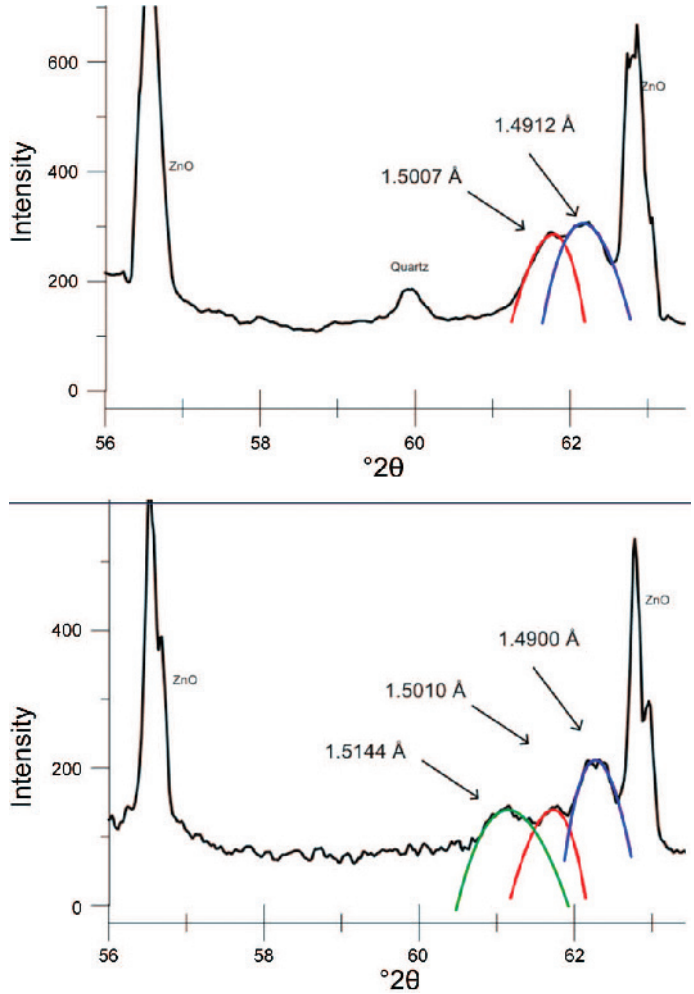

Figure 9. (upper) Decomposition of the 060 area of the clay samples; (lower) decomposition of the 060 area for sand samples. The blue curve represents the contribution from kaolinite; the red curve represents the contribution from all dioctahedral Al-clays (smectite, illite, illite-smectite) while the green curve corresponds to the contribution of glauconite and/or glauconite-smectite. XRD patterns were recorded with ZnO as the reference material.

Finally, the clay mineralogy of the estuarine Mol sands consisted mainly of kaolinite but also contained clay-sized glauconite in significant amounts. Note that these quartz-rich sands contained glauconite pellets only in their clay fraction; clay-sized glauconite represents an important proportion of the clay fraction. Only the less expandable clay-sized glauconite type was necessary to model the clay fractions of the Mol Formation

Clays. Sedimentary clay samples were examined in all lithological units. In contrast to the sand samples, the <2 μm clay fractions displayed brown to grey coloration. The XRD patterns of clays were similar to those of sand samples, and modeled clay mineral characteristics were identical to those in sands. Inspection of the d_{060} of randomly oriented powders, however, indicated that clay-sized glauconite was systematically absent from clays (Figure 9, Table 4). This was confirmed by the clay modeling because oriented clay patterns could not be modeled with the incorporation of Fe-rich clay minerals (Figure 8). The most important clay minerals in these size fractions were dioctahedral Al-smectite, Al-rich illite-smectite, kaolinite, and chlorite (Table 4).

DISCUSSION

Clay-sized glauconite was encountered systematically in Cenozoic marine glauconite pellet-bearing samples. Both the experiments and the data presented reveal that inappropriate use of laboratory treatments can cause glauconite pellet disintegration. However, after removing the >32 μm glauconite pellets, the amount of contaminated clay-sized glauconite was at most 25% and the real value is probably much less. Therefore, most of the clay-sized glauconite must have a natural origin. Its presence is confirmed in units that contain glauconite pellets which were probably less transported or even authigenic but also in units where

https://doi.org/10.1346/CCMN.2014.0620104 Published online by Cambridge University Press

Table 4. Quantitative clay mineralogy of each analyzed sample. Glauconite contents are shown for sand samples together with d_{060} values of both pelletal and clay-sized glauconite. Question marks indicate that the exact 060 position could not be determined due to low glauconite abundance in the particular sample.

Sample	Formation	Glauconite grains 060 (Å)	Glauconite clay 060 (Å)	% Glauconite grains in the >32 μm fraction	Kaolinite	Illite	Mixed layer illite-smectite	Clay-sized glauconite (less expandable)	Clay-sized glauconite (more expandable)	Di-smectite	Tri-smectite	Chlorite
B1	Berchem	1.5139	1.5144	40	4	8	22	3	13	50	0	1
B2	Berchem	1.5139	1.5139	32	5	14	13	2	13	51	0	1
B3	Berchem	1.5144	1.5139	29	2	4	29	3	7	55	0	1
B4	Berchem	1.5148	1.5135	34	4	4	36	7	11	37	0	1
B5	Berchem	1.5148	1.5144	36	1	5	32	3	14	44	0	1
B6	Berchem	1.5139	1.5131	39	5	5	17	1	18	54	0	1
B7	Berchem	1.5128	1.5153	43	1	7	26	10	13	42	0	1
B8	Berchem				10	14	48	0	0	27	0	1
B9	Berchem				10	13	48	0	0	29	0	1
B10	Berchem	1.5139	1.5135	35	3	3	38	6	15	35	0	1
B11	Berchem	1.5144	1.5131	43	5	5	33	0	2	54	0	1
B12	Berchem	1.5148	1.5144	48	7	17	33	4	10	28	0	1
B13	Berchem	1.5139	?	55	1	5	34	5	12	42	0	1
				0			0					
D1	Diest	1.5153	1.5157	20	6	17	25	27	17	7	0	1
D2	Diest	1.5148	1.5162	27	5	10	30	32	13	9	0	1
D3	Diest	1.5148	1.5157	20	5	10	27	34	15	7	0	2
D4	Diest	1.5162	1.5171	19	15	18	26	30	8	2	0	1
D5	Diest	1.5180	1.5175	38	5	4	33	4	18	15	21	0
D6	Diest				28	14	26	0	0	31	0	1
D7	Diest	1.5189	1.5189	31	2	3	5	90	0	0	0	0
D8	Diest	1.518	1.5189	32	1	6	10	84	0	0	0	0
D9	Diest	1.518	1.518	36	2	2	22	72	0	1	0	1
D10	Diest	1.5189	1.5184	35	1	0	3	96	0	0	0	0
D11	Diest				19	18	29	0	0	34	0	1
D12	Diest				21	12	35	0	0	31	0	1
				0			0					
K1	Kasterlee	1.5166	1.5162	6	18	4	16	51	10	0	0	1
K2	Kasterlee	1.5166	1.5166	6	24	5	44	17	5	4	0	1
K3	Kasterlee	1.5171	1.518	5	25	10	17	34	9	4	0	1
K4	Kasterlee	1.5162	1.5166	5	20	8	19	20	26	6	0	1
K5	Kasterlee	1.5166	1.5171	5	18	6	19	28	23	5	0	1
K6	Kasterlee				34	19	39	0	0	7	0	1
K7	Kasterlee				30	15	42	0	0	12	0	1
				0								
M1	Mol		1.5135	0	45	7	14	34	0	0	0	0
M2	Mol		1.5144	0	48	8	13	31	0	0	0	0
M3	Mol		1.5148	0	49	8	12	31	0	0	0	0
M4	Mol		1.5139	0	48	12	10	30	0	0	0	0
M5	Mol		1.5135	0	47	11	12	30	0	0	0	0
P1	Poederlee	1.5222	1.5238	20	14	15	18	4	12	18	17	2
P2	Poederlee	1.5211	1.522	24	16	18	16	5	9	15	19	2
P3	Poederlee	1.522	?	22	16	17	22	2	4	20	17	2
P4	Poederlee	1.5211	?	21	17	14	21	2	2	28	16	0
P5	Poederlee	1.5202	?	24	11	6	16	0	0	32	33	2
P6	Poederlee	1.5202	?	22	9	5	12	0	3	38	33	1

glauconites were transported in the same way as the detrital quartz (Figure 4). Furthermore, the occurrence of the glauconite pellets is not restricted to marine glauconite pellet-bearing units because the estuarine Mol Formation also contains clay-sized glauconite.

The relation between clay-sized glauconite and pelletal glauconite

The occurrence of clay-sized glauconite was reported by Baioumy and Boulis (2012) who suggested a pre-pelletal stage in the glauconitization process. The occurrence of fine-grained glauconite is indeed expected in areas where new glauconite pellets are being formed (Odin, 1982). Clay-sized glauconite is, however, rarely reported coexisting with sand-sized glauconite pellets. If reported, the clay fraction of early-stage or more evolved glauconitic sediments typically consists of Al-rich clay minerals (Bell and Goodell, 1967; Seed, 1968; Baldermann *et al.*, 2012) and rarely of Fe-rich clays.

In the current case, however, the results illustrate glauconite occurrence in sand and clay fractions, which both display a very similar two-phase glauconite-smectite R1 mineralogy (Table 4). The near-linear relation between d_{060} values of glauconite pellets and clay-sized glauconite in the same sample (Figure 10) demonstrates the close association between both glauconite types. Furthermore, d_{060} values can be used as a parameter to distinguish the different analyzed formations (Figure 10), which supports the idea that both sand-sized and clay-sized glauconite occurrences are closely related. While during clay modeling an identical glauconite-smectite R1 structure was used to model both the clay-sized and the pelletal glauconite, the respective d_{060} values are not always identical (Figure 10). However, compositional differences exist between the outer and inner surfaces of glauconite pellets, as well as between larger and smaller glauconite pellets (Harris *et al.*, 2007), which could explain such small-scale mineralogical differences Nevertheless, the interpretation is, then, that both glauconite types indeed belong to the same system but occur in different sizes.

The origin of clay-sized glauconite in marine deposits

When assuming that both glauconite types are part of the same system, this must mean that either pellet disaggregation or pelletization of clay-sized glauconite is the controlling process. An alternative hypothesis is that both types were formed simultaneously.

El Albani (2005) and Banerjee *et al.* (2012) demonstrated that glauconite authigenesis results in distinct mineralogical and crystal-chemical differences between different glauconite types, which is clearly not observed in the present setting

Furthermore, if the clay-sized glauconite is an authigenic precipitate, this should be reflected in its properties as the process of glauconitization depends on the amount of available Fe and, thus, the prevailing redox conditions (Odin, 1982; Chamley, 1989). El Albani (2005) demonstrated that open marine conditions yield the anoxic conditions necessary for Fe mobility through organic matter resulting in a large amount of Fe and K uptake in the glauconite structure. Near-coastal or estuarine environments are, on the contrary, influenced

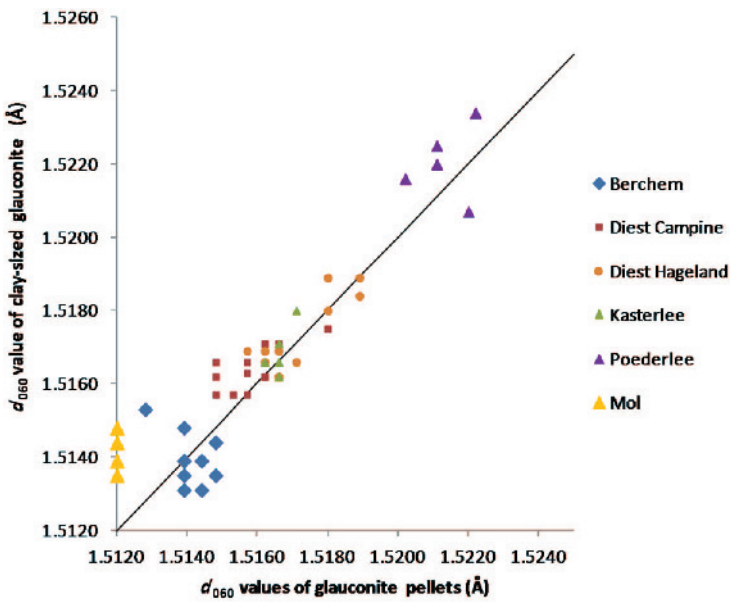

Figure 10. Glauconite pellet d_{060} values plotted against clay-sized glauconite d_{060} values, following a 1:1 relation. The d_{060} value is apparently a good parameter to distinguish between different formations. The yellow line indicates the position of the clay-sized glauconite of the Mol formation.

https://doi.org/10.1346/CCMN.2014.0620104 Published online by Cambridge University Press

by oxic freshwaters which will strongly reduce the amount of available Fe and result in Al-rich glauconites with d_{060} spacings of between 1.50 Å and 1.51 Å (Parry and Reeves, 1966; Porrenga, 1968; Berg-Madsen, 1983; El Albani *et al.*, 2005). Louwye (2005) and Louwye *et al.* (2006) found evidence for near-coastal depositional environments with continental influences in the Kasterlee and Poederlee Formations, while the Berchem and Diest Formations were exposed to fully marine conditions. The quartz sands of the Mol Formation were deposited in estuarine conditions (Vandenberghe *et al.*, 1998). The mineralogy and crystal chemistry of the clay-sized glauconite found in these units (Table 4) revealed little correspondence with a sedimentary environment, as the Fe contents are almost equal in each of the formations described. Although anoxic conditions may also develop in near coastal environments (Gertsch *et al.*, 2010; Wignall and Newton, 2001), this involves large amounts of organic material and is not found in the current deposits.

Baioumy and Boulis (2012) suggested that clay-sized glauconite can form pellets at a later stage due to reworking or circulation processes. This seems rather unlikely in the current situation because clay-sized and pelletal glauconite occur systematically together in the same system and, furthermore, are never present in intercalated clay layers. Moreover, based on d_{060} values and, thus, Fe-contents and K_2O-values of the glauconite pellets (Table 3), both types of glauconite represent well evolved glauconitization stages which contradicts an early-stage origin. Considering that the bulk of pelletal glauconites was actively transported (Figure 4), and that both pelletal and clay-sized glauconite are probably part of the same system, a true authigenic nature of the clay-sized glauconite is, therefore, very unlikely.

The only stratigraphic occurrence where clay-sized glauconite has been reported coexisting with glauconite pellets are soils and weathering profiles (Van Ranst and De Coninck, 1983; Tedrow, 1986, 2002). In this case, the characteristics of both glauconite types are expected to be equal because clay-sized glauconite formation is related to weathering and soil processes (Velde and Meunier, 2008). In the current setting, however, soil environments are excluded. Considering the limited depth of burial and the fact that glauconite pellets are not deformed, compaction is also to be excluded. The origin of the clay-sized glauconite is probably related to the abrasion and breaking up of glauconite pellets during physical transport.

A key observation is that clay-sized glauconite is incorporated in the clay fraction of sands but never in the intercalated clay layers (Table 4, Figure 8). The type and relative proportions of clay minerals in both sands and clays are very similar, indicating that Al-smectite, Al-rich illite-smectite, illite-smectite, kaolinite, and chlorite mainly originate from a detrital source area. This clay assemblage probably constitutes the 'background' clay mineralogy in sands and clays but apparently does not include clay-sized glauconite. Furthermore, no linear relation exists between clay-sized glauconite and the detrital sedimentary clay fraction (Figure 11). As a result, a distant source area is excluded as the main source of clay-sized glauconite but points to a more local origin. A physically weaker population of incomplete or broken glauconite pellets of older deposits was probably abraded over short-range transport or decomposed on impact.

This process of abrasion of glauconite pellets into a clay-sized glauconite fraction is most logical in glauconite pellet-bearing sediments for which the glauconite pellets are apparently transported together with the detrital, mainly quartz, fraction (Figure 4). Although the Poederlee and Antwerp sands favor glauconite pellet authigenesis (Figure 4; see also Odin *et al.*, 1974), clay-sized glauconite is also present in these deposits, which seems to contradict a transported origin (Table 4). The heterogeneity in glauconite-pellet size distribution (Figure 4), however, suggests that a variety of depositional processes played an important role, indicating that glauconite pellets are not exclusively authigenic. Glauconite pellets in these units were, therefore, only transported over short distances as they were swept over the shelf during transgressive movement away from the area of glauconitization. This process is apparently sufficient to produce clay-sized glauconite but in smaller amounts than detrital glauconite pellets. Consequently, the amount of clay-sized glauconite can be used as a proxy for the amount and intensity of pelletal glauconite transport and the energy of the depositional environment. This is demonstrated by the small amounts of clay-

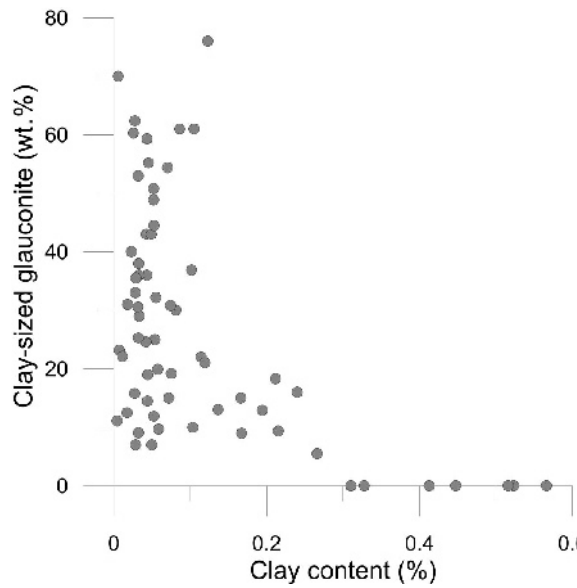

Figure 11. The <2 µm clay fraction plotted *vs.* the amount of <2 µm glauconite which shows no linear relation.

https://doi.org/10.1346/CCMN.2014.0620104 Published online by Cambridge University Press

sized glauconite in the Poederlee sands, and, to a lesser degree, the Antwerp sands (Table 4).

The origin of clay-sized glauconite in the estuarine Mol Formation

The estuarine Mol sands are very mature sands with no glauconite pellets and the 30% clay-sized glauconite in its clay fraction (Table 4). The clay-sized glauconite in these sands cannot, therefore, be derived from pre-existing pelletal glauconite in the Mol Formation. The estuarine environment in which this deposit was formed does not yield the necessary reducing conditions for glauconitization which makes an authigenic origin unlikely. Estuarine glauconitization was reported by El Albani (2005) but the amount of Fe incorporated in those mineral structures was much less than the relatively large Fe contents found in the clay-sized glauconite of the Mol Formation. Nevertheless, clay-sized glauconite produced in slightly older deposits can be further taken up in subsequent erosion and sedimentation cycles together with clays from other sources. The clay-sized glauconite in the estuarine Mol Formation must, therefore, be reworked from the locally out-cropping glauconitic sands occurring in and around the estuary (Figures 2, 3). The d_{060} position of the Mol sands (Figure 10) is, however, slightly different from the older Kasterlee and Poederlee Formations, suggesting that Fe is lost from the clay-mineral structure during transport or as the result of acid percolation, leading to a slightly more Al-rich glauconite mineralogy.

Significance of expandable minerals

The abundance of expandable minerals in the clay fraction of the glauconitic sediments (Table 4) could indicate that it is the precursor of glauconite minerals as suggested by Buatier *et al.* (1989) and Jimenez-Millan *et al.* (1998). Clay modeling of the dioctahedral smectite, present in almost all the formations described, resulted in octahedral Fe contents of 0.05−0.25/half unit cell, common values for Al-rich dioctahedral smectites (Güven, 1988).

In the Poederlee Formation, however, a trioctahedral expandable phase is also present. Clay modeling resulted in an octahedral Fe content of ~1.5/half unit cell, which is significantly greater than the 0.75–0.9 octahedral Fe cations/half unit cell typical of glauconite pellets and clay-sized glauconite in these sediments. This Fe-rich expandable phase is also present in the glauconite pellets of the Poederlee Formation (Figure 7, Table 4), illustrating the mineralogical relation between glauconite pellets and the associated clay fraction. Furthermore, size distributions of the glauconite pellets (Figure 4) and the small amounts of clay-sized glauconite (Table 4) demonstrate that glauconitization took place at a nearby area or even partially at the current position. Nevertheless, the Fe-expandable phase in this particular deposit is probably the precursor mineral which induced pelletal glauconitization.

CONCLUSIONS

Experiments show that the large majority of clay-sized glauconite is naturally present in the samples. However, certain populations of glauconite particles tend to break up during strong physical actions of the sediment, excessive shaking at high speeds, and during standard clay preparations. This effect can be strongly reduced by isolating >32 μm glauconite particles prior to further clay mineralogical preparations. The data presented prove the existence of natural clay-sized glauconite in Neogene glauconite pellet-bearing and non-glauconite pellet-bearing sand deposits in the northern part of Belgium. The origin of clay-sized glauconite is not authigenic but related to glauconite pellet abrasion and disintegration upon transport. Intercalated sedimentary clay layers of the same deposits were never found to incorporate the clay-sized glauconite, meaning that the latter did not originate from distant detrital source areas but rather has a local origin within the same depositional basin. The amount of clay-sized glauconite produced is indicative of the distance and intensity of transport. The clay-sized glauconite in the estuarine Mol Formation was derived by erosion of older deposits around the estuary and reworked. A trioctahedral Fe-rich expandable phase was identified in both the clay fraction and the glauconite pellets of the Poederlee sands, suggesting that it acted as the precursor mineral for pelletal glauconitization. Clay-sized glauconite has never been reported as such before and is clearly an important contributor to the clay fraction in these deposits, emphasizing the energetic character of the environment in which they were formed.

REFERENCES

Adriaens, R. (2009) Mineralogical and crystal-chemical analysis of glauconites in the Upper-Cretaceous and Cenozoic strata of the Southern North Sea basin. Unpublished Masters thesis, University of Leuven, Leuven, Belgium, 105 pp.

Amorosi, A. (1995) Glaucony and sequence stratigraphy: a conceptual framework of distribution in siliciclastic sequences. *Journal of Sedimentary Research*, **65**, 419−425.

Amorosi, A. (1997) Detecting compositional, spatial, and temporal attributes of glaucony: a tool for provenance research. *Sedimentary Geology*, **109**, 135−153.

Bailey, S.W. (1980) Summary of recommendations of AIPEA nomenclature committee. *Clays and Clay Minerals*, **28**, 73−78.

Bailey, S.W. (1988) *Hydrous Phyllosilicates (exclusive of Micas)*. Reviews in Mineralogy, **19**, Mineralogical Society of America, Washington, D.C., 725 pp.

Baioumy, H. and Boulis, S. (2012) Non-pelletal glauconite from the Campanian Qusseir Formation, Egypt: Implication for glauconitisation. *Sedimentary Geology*, **249**, 1−9.

Baldermann, A., Grathoff, G.H., and Nickel, C. (2012) Micromileu-controlled glauconitisation in fecal pellets at Oker (Central Germany). *Clay Minerals*, **47**, 513−538.

Banerjee, S., Jeevankumar, S., and Eriksson, P.G. (2008) Mg-rich ferric illite in marine transgressive and highstand systems tracts: examples from the Paleoproterozoic Semri

https://doi.org/10.1346/CCMN.2014.0620104 Published online by Cambridge University Press

Group, central India. *Precambrian Research*, **162**, 212–226.
Banerjee, S., Chattoraj, S.L., Saraswati, P.K., Dasgupta, S., and Sarkar, U. (2012) Substrate control on formation and maturation of glauconites in the Middle Eocene Harudi Formation, western Kutch, India. *Marine and Petroleum Geology*, **30**, 144–160.
Bell, D.H. and Goodell, H.G. (1967) A comparative study of glauconite and the associated clay fraction in modern marine sediments. *Sedimentology*, **9**, 169–202.
Berg-Madsen, V. (1983) High-alumina glaucony from the middle Cambrian of Öland and Bornholm, Southern Baltoscandia. *Journal of Sedimentary Petrology*, **53**, 875–893.
Buatier, M., Honnorez, J., and Ehret, G. (1989) Fe-smectite-glauconite transition in hydrothermal green clays from the Galapagos spreading center. *Clays and Clay Minerals*, **37**, 532–541.
Buckley, H.A., Bevan, J.C., Brown, K.M., Johnson, L.R., and Farmer, V.C. (1978) Glauconite and celadonite: two separate mineral species. *Mineralogical Magazine*, **42**, 373–382.
Chafetz, H.S. and Reid, A. (2000) Syndepositional, shallow water precipitation of glauconitic minerals. *Sedimentary Geology*, **136**, 29–42.
Chamley, H. (1989) *Clay Sedimentology*. Springer-Verlag, Berlin, 623 pp.
Cudzil, M.R. and Driese, S.G. (1987) Fluvial, tidal and storm sedimentation in the Chilhowee Group (Lower Cambrian), northeastern Tennessee, U.S.A. *Sedimentology*, **34**, 861–883.
De Meuter, F.J. and Laga, P. (1976) Lithostratigraphy and biostratigraphy based on benthonic foraminifera of the Neogene deposits of northern Belgium. *Bulletin de Société belge Géologie*, **85**, 133–152.
Derkowski, A., Środoń, J., Franus, J., Uhlík, P., Banaś, M., Zieliński, G., Čaplovičova, M., and Franus, M. (2009) Progressive dissolution of glauconite and its implications for the methodology of K-Ar and Rb-Sr dating. *Clays and Clay Minerals*, **57**, 531–554.
Eberl, D.D., Środoń, J., Lee, M., Nadeau, P.H., and Northrop, H.R. (1987) Sericite from the Silverton caldera, Colorado: Correlation among structure, composition, origin, and particle thickness. *American Mineralogist*, **72**, 914–934.
El Albani, A. (2005) Unusual occurrence of glauconite in a shallow lagoonal environment (Lower Cretaceous, northern Aquitaine Basin, SW France). *Terra Nova*, **17**, 537–544.
Gertsch, B., Adatte, T., Keller, G., Aziz, A.M., Tantawy, A., Berner, Z., Mort, H.P., and Fleitmann, D. (2010) Middle and late Cenomanian oceanic anoxic events in shallow and deeper shelf environments of western Morocco. *Sedimentology*, **57**, 1430–1462.
Gonzalez, R., Dias, J.M.A., Lobo, F., and Mendes, I. (2004) Sedimentological and paleoenvironmental characterization of transgressive sediments on the Guadiana Shelf (Northern Gulf of Cadiz, SW Iberia). *Quaternary International*, **120**, 133–144.
Güven, N. (1988) Smectites. Pp 497–559 in: *Hydrous Phyllosilicates*. Reviews in Mineralogy, **19**. Mineralogical Society of America, Washington DC.
Harris, W.B., Fullager, P.D., and Tovo, L.T. (2007) Significance of young Paleocene Rb-Sr glauconite dates from the Lang Syne Formation, Savannah River site, South Carolina. *Southeastern Geology*, **37**, 55–72.
Hesselbo, S.P. and Huggett, J.M. (2001) Glaucony in ocean-margin sequence stratigraphy (Oligocene–Pliocene, Offshore New Jersey, USA; ODP Leg 174A). *Journal of Sedimentary Research*, **71**, 598–606.
Ireland, B.J., Curtis, C.D., and Whiteman, J.A. (1983) Compositional variation within some glauconites and illites and implications for their stability and origins. *Sedimentology*, **30**, 769–786.
Jackson, M.L. (1975) *Soil Chemical Analysis – Advanced Course*, 2nd edition. Published by the author, Madison, Wisconsin, USA, 895 pp.
Jimenez-Millan, J., Molina, J.M., Nieto, F., Nieto, L., and Ruiz-Ortiz, P.A. (1998) Glauconite and phosphate peloids in Mesozoic carbonate sediments (Eastern Subbetic Zone, Betic Cordilleras, SE Spain). *Clay Minerals*, **33**, 547–559.
Kleeberg, R. (2005) Results of the second Reynolds Cup contest in quantitative mineral analysis. International Union of Crystallography. *Commission on Powder Diffraction Newsletter*, **20**, 22–24.
Louwye, S. (2001) New species of dinoflagellate cysts from the Berchem formation, Miocene, northern Belgium (southern North Sea basin). *Geobios*, **34**, 121–130.
Louwye, S. (2005) The Early and Middle Miocene transgression at the southern border of the North Sea Basin (northern Belgium). *Geological Journal*, **40**, 441–456.
Louwye, S. and De Schepper, S. (2010). The Miocene–Pliocene hiatus in the southern North Sea Basin (northern Belgium) revealed by dinoflagellate cysts. *Geological Magazine*, **5**, 760–776.
Louwye, S. and Laga, P. (1998) Dinoflagellate cysts of the shallow marine Neogene succession in the Kalmthout well, northern Belgium. *Bulletin of the Geological Society of Denmark*, **45**, 73–86.
Louwye, S., De Coninck, J., and Verniers, S. (1999) Dinoflagellate cyst stratigraphy and depositional history of Miocene and Lower Pliocene formations in northern Belgium (southern North Sea basin). *Geologie en Mijnbouw*, **78**, 31–46.
Louwye, S., De Conick, J., and Verniers, J. (2000) Shallow marine Lower and Middle Miocene deposits at the southern margin of the North Sea Basin (northern Belgium): dinoflagellate cyst biostratigraphy and depositional history. *Geological Magazine*, **137**, 381–394.
Louwye, S., De Schepper, S., Laga, P., and Vandenberghe, N. (2006) The Upper Miocene of the southern North Sea Basin (northern Belgium): a palaeoenvironmental and stratigraphical reconstruction using dinoflagellate cysts. *Geological Magazine.* **144**, 33–52.
Maréchal, R. (1994) A new lithostratigraphic scale for the Palaeogene of Belgium. *Bulletin de la Société belge de Géologie*, **102**, 215–229.
McRae, S.C. (1972) Glauconite. *Earth-Science Reviews*, **8**, 397–440.
Meunier, A. (2005) *Clays*. Springer-Verlag, Berlin, 472 pp.
Meunier, A. and El Albani, A. (2007) The glauconite-Fe-illite-Fe-smectite problem: a critical review. *Terra Nova*, **19**, 95–104.
Moore, D.M. and Reynolds, R.C. Jr. (1997) *X-ray Diffraction and the Identification and Analysis of Clay Minerals*, second edition. Oxford University Press, Oxford, New York, 371 pp.
Odin, G.S., (1982) *Numerical Dating in Stratigraphy.* Wiley Interscience, New York, 1094 pp.
Odin, G.S. and Fullager, P.D. (1988) Geological significance of glaucony facies. Pp. 295–332 in: *Green Marine Clays* (G.S. Odin, editor). Developments in Sedimentology, **45**, Elsevier, Amsterdam.
Odin, G.S. and Matter, A. (1981) De glauconiarum origine. *Sedimentology*, **28**, 611–641.
Odin, G.S., Hunziker, J.C., Keppens, E., Laga, P.G., and Pasteels, P. (1974) Analyse radiométrique de glauconies par les méthodes au strontium et a l'argon; L'Oligo-Miocène de Belgique. *Bulletin de Société belge Géologie*, **83**, 35–48.
Omotoso, O., McCarthy, D.K., Hillier, S., and Kleeberg, R. (2006) Some successful approaches to quantitative mineral

analysis as revealed by the 3rd Reynolds Cup contest. *Clays and Clay Minerals*, **54**, 748–760.

Parry, W.T. and Reeves, Jr., C.C. (1966) Lacustrine glauconitic mica from Pluvial Lake Mound, Lynn and Terry Counties, Texas. *American Mineralogist*, **51**, 229–235.

Porrenga, D.H. (1968) Non-marine glauconitic illite in the Lower Oligocene of Aardebrug, Belgium. *Clay Minerals*, **7**, 421–430.

Potter, P.E., Maynard, B.J., and Depetris, J.P. (2005) *Mud and Mudstones*. Springer-Verlag, New York, 297 pp.

Sakharov, B.A., Lindgreen, H., Salyn, A.L., and Drits, V.A. (1999) Determination of illite-smectite structures using multispecimen X-ray diffraction profile fitting. *Clays and Clay Minerals*, **47**, 555–566.

Seed, D.P. (1968) The analysis of the clay content of some glauconite oceanic sediments. *Journal of Sedimentary Petrology*, **38**, 229–231.

Środoń, J., Drits, V.A., McCarty, D.K., Hsieh, J.C.C., and Eberl, D.D. (2001) Quantitative XRD analysis of clay-rich rocks from random preparations. *Clays and Clay Minerals*, **49**, 514–528.

Tedrow, J.C.F. (1986) *Soils of New Jersey*. Robert E. Krieger Publishing Company, Malabar, Florida, USA, 479 pp.

Tedrow, J.C.F. (2002) *Greensand and Greensand Soils of New Jersey: a review.* Department of Ecology, Evolution and Natural Resources Rutgers University, New Brunswick, New Jersey, USA, 40 pp.

Udgata, D.B.P. (2007) Glauconite as an indicator of sequence stratigraphic packages in a lower Paleocene passive-margin shelf succession, Central Alabama. Masters thesis, Auburn University, Alabama, USA, 124 pp.

Van Ranst, E. and De Coninck, F. (1983) Evolution of glauconite in imperfectly drained soils of the Belgian Campine. *Zeitschrift fur Pflanzenernahrung und Bodenkunde*, **146**, 415–426.

Vandenberghe, N., Laga, P., Steurbaut, E., and Vail, P.R. (1998) Tertiary sequence stratigraphy at the southern border of the North Sea basin in Belgium. *Mesozoic and Cenozoic Sequence Stratigraphy of European Basins*. SEPM special publication No **60**, pp. 119–154, Society for Sedimentary Geology, Tulsa, Oklahoma, USA.

Vandenberghe, N., Van Simaeys, S., Steurbaut, E., Jagt, J., and Felder, P. (2004) Stratigraphic architecture of the Upper Cretaceous and Cenozoic along the southern border of the North Sea Basin in Belgium. *Netherlands Journal of Geosciences-Geologie en Mijnbouw*, **83**, 155–171.

Velde, B. (1985) *Clay Minerals*. Developments in Sedimentology, **40**. Elsevier, Amsterdam, 427 pp.

Velde, B. and Meunier, A. (2008) *The Origin of Clay Minerals in Soils and Weathered Rocks*. Springer Verlag, Berlin, 406 pp.

Weaver, C.E. and Pollard, L.D. (1973) *The Chemistry of Clay Minerals*. Developments in Sedimentology, **15**, Elsevier Scientific Publishing Company, Amsterdam, London, New York, 213 pp.

Wignall, P.B. and Newton, R.J. (2001) Black shales on the basin margin: a model based on examples from the Upper Jurassic of the Boulonnais, northern France. *Sedimentary Geology*, **144**, 335–356.

Wilson, A.D. (1955) A new method for the determination of ferrous iron in rocks and minerals. *Bulletin of the Geological Survey of Great Britain*, **9**, 56–58.

Zeelmaekers, E. (2011) Computerized qualitative and quantitative clay mineralogy: Introduction and application to known geological cases. Doctoral dissertation, University of Leuven, Leuven, Belgium, 397 pp.

(*Received 2 July 2013; revised 2 February 2014; Ms 785; AE: H. Dong*)